THE JOURNAL OF Ammonia Energy

Available online at

jae.cardiffuniversitypress.org

ISSN **2752-7735**
The Journal of Ammonia Energy 02 (2024) 085–100

Cardiff University Press | Gwasg Prifysgol Caerdydd

An Indirect Ammonia Fuelled Solid-Oxide Fuel Cell System with free cracking from Waste Heat

Peters BM*, Huddart AD, Cowan R, Smith J and Davenne T

*Science and Technology Facilities Council, Rutherford Appleton Laboratory, Oxfordshire, United Kingdom

Abstract

A 100W scale indirect ammonia solid oxide fuel cell (IA-SOFC) system called REACH was designed, built and tested at the Rutherford Appleton Laboratory, with an off-the-shelf 100W solid oxide fuel cell at its core. IA-SOFCs with thermal integration of cracking have been modelled at a large scale, and there have been single cell studies focusing on the degradation and NOx emissions while running on ammonia. REACH addresses the gap of demonstrating an integrated system and only a few stack-scale demonstrators to have been tested in academia. The purpose of this work was to present an engineering design that demonstrates the practical possibilities of using the waste heat from high-temperature SOFCs to perform ammonia cracking, and to demonstrate a real-world efficiency of above 45% for such a system. Tests were conducted in a fume hood with gaseous supplies of air and ammonia. The start-up testing proved that the proposed design is capable of autothermal cracking. The performance mapping of the fuel cell, that is the sweeping of fuel rates at differing air-fuel ratios, revealed a system efficiency of 14%. Upon diagnosis, this was due to low fuel utilisation of the off-the-shelf SOFC at its intended operating condition, which the supplier's anode reduction process is likely to have caused. This illustrated that the commercial availability of reliable SOFC stacks can be an obstacle to research in this field. However, an effective design was delivered that has practically demonstrated the use of waste heat and unconverted fuel to pre-crack for high temperature SOFCs (autothermal cracking without power input for heating), thus a direct ammonia to power system that avoids the need for upstream purification steps was delivered. Questions remain around the precise composition of its exhaust, and suggestions for a follow up prototype are to remove the vacuum vessel and scale-up the power rating of the system to the 1-10kW scale.

Received: 8th Mar 24; Accepted: 22nd Jun 24; Published: 4th Jul 24

Keywords: indirect ammonia fuel cell, solid oxide fuel cell, IA-SOFC, autothermal, integrated ammonia cracking, prototype, testing.

Introduction

Fuel cell systems are a promising method for converting the potentially net-zero compatible energy vector, ammonia, to electrical power. The advantages such systems pose over internal combustion or gas turbine ammonia conversion solutions have been reported as: higher achievable efficiencies not limited by the Carnot cycle, their energy is clean and free of nitrous oxide (NOx) emissions, their efficiency is independent of plant scale, and they are modular [1]. We would only amend these statements to say that there is the *potential* for zero NOx emissions and that demonstrators must monitor the outputs to be sure.

There are numerous ways in which ammonia has been used with fuel cells. Indirect ammonia fuel cells (IA-FCs) have an upstream cracker (decomposition reactor) such that cracked ammonia or pure hydrogen enters the fuel cell. One configuration of IA-FC is to couple with the most mature hydrogen fuel cell technology, Polymer Electrolyte Membrane (PEM) fuel cells. Due to maturity and commercial availability, the approach has underpinned the greatest real-world successes so far; PEM with external decomposition and purification has been demonstrated by AMOGY on some heavy vehicles [2]. However, there are some significant caveats with this approach. Firstly, there is a heavy reliance on purification with purity requirements of <0.1 ppm NH_3 being required to not seriously damage the PEM cells [3, 4]. *Absorbent bed* purifiers are inherently complex and expensive because the beds need replacing once they become saturated with contaminants, or they require purging in a cyclic batch process [5]. A leading *continuous filter* option, palladium membrane purification, requires careful temperature control and can suffer from degradation and pinhole leaks [6].

Direct ammonia fuel cells (DA-FCs) are researched due to the potential simplicity of avoiding the requirement for ammonia decomposition, or as we will refer to it from now on, ammonia *cracking*. Direct ammonia alkaline fuel

* Corresponding author. Tel.: +44-1235-446106. E-mail address: benjamin.peters@stfc.ac.uk
https://doi.org/10.18573/jae.33

cells (DA-AFCs) have been proven to operate on ammonia directly at low temperatures (<100ºC), but a review on the progress of this technology shows that they are still considerably below the power densities of hydrogen-fed fuel cells; typically, around 10 mW/cm^2 versus the 500 mW/cm^2 of PEM [7].

Solid oxide fuel cells (SOFCs) occupy an interesting middle ground, with potential for IA-FC and DA-FC configuration due to their tolerance of ammonia and nitrogen. Furthermore, due to high-temperature operation (typically above 600ºC), there is high-grade heat available for supporting ammonia cracking. In fact, there is an ongoing debate on whether it is a good or bad idea to configure SOFCs as DA-SOFCs, which is possible because the ammonia will simply crack upon entry to the high temperature environment of the SOFC. There are advocates [8], and those revealing high thermal stresses associated with thermal cold-spots created by the decomposition endotherm [9]. A laboratory demonstrator was built in Korea to test and compare the same 1kW stack configured as a DA-FC and IA-FC [10]. This study revealed good performance in both configurations, with some drop in temperature noted when directly fueled with ammonia. Post-mortem analysis showed that the DA-FC configuration was resulting in nitriding, which although was not a problem for 1000 hours, was thought to be a problem in the long-term. With this in mind, we set about the design of a novel IA-SOFC system.

The focus of this paper is to detail a prototype named REACH, which stands for Renewable Energy Ammonia Charging. This backronym implies suitability for the decarbonization of remote, off-grid locations, which is why it was styled after a back-up generator. It is an indirect ammonia solid-oxide fuel cell system with external thermally coupled cracking (a thermally coupled IA-SOFC). REACH follows the "autothermal decomposition configuration" of Kishimoto's 2020 publication [10] but with thermal and mechanical design innovations that facilitate robust autothermal operation with a compact footprint. The innovation is a manufacturable design that incorporates a heat-exchanger with integrated cracker (the critical link between waste heat and the incoming ammonia and air), and a catalytic combustor (to put residual fuel to good use, intended especially for the start-up).

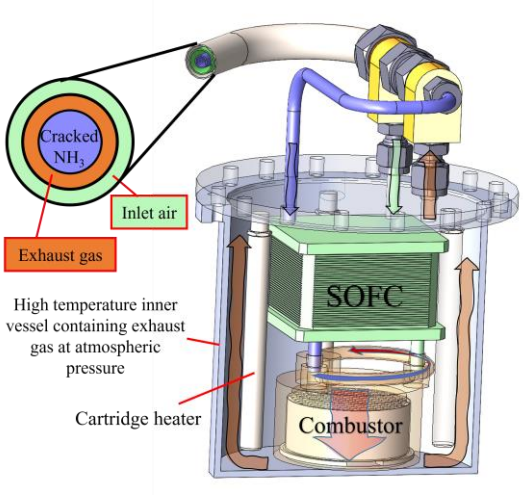

Fig. 1. Preliminary design of inner vessel.

REACH is designed around a commercially available 100W SOFC, seen at the heart of Fig. 1. We introduced a catalytic combustor after the SOFC so that both devices would sit within a high-temperature chamber, and a heat exchanger with integrated cracker that can obtain all the heat it needs for cracking from the exhaust gases of the high temperature chamber. The catalytic combustor performs the function of being ready to convert unspent fuel from the SOFC from 400 ºC upwards. This provides the chance to use the fuel to help heat the SOFC during start up, get the maximum amount of useful heat from the calorific content of the fuel by extracting what remains after the SOFC, and "clean up" residual hydrogen and ammonia that have global warming potential and toxicity issues respectively. As shown in the preliminary design in Fig. 2, the inner vessel and heat exchanger with integrated cracker were situated inside an outer vessel designed to ensure the overall heat loss was low enough to facilitate autothermal operation.

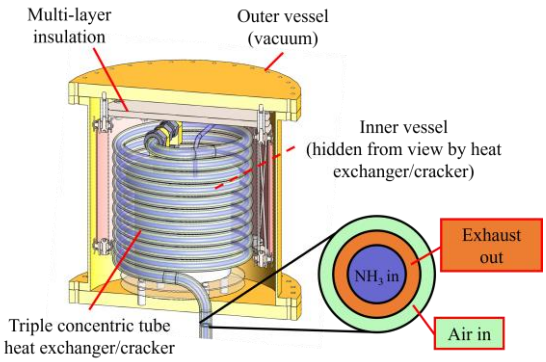

Fig. 2. Preliminary design of outer vessel.

The REACH design is an attempt to increase the technology readiness by creating a transportable, plug and play unit. The research questions we wanted to answer are: does this IA-SOFC concept work at 100W scale? What are the engineering challenges of such a system in practice? This is primarily a report of the design and test of our work which successfully demonstrated the concept at the scale. Finally, before proceeding to the main body of our work, a note on NOx emissions from SOFCs. A recent study has rightly pointed out that IA-SOFCs and DA-SOFCs can form NOx emissions if the SOFC is based on oxygen-transfer [11]. The SOFC inside REACH is based on oxygen-transfer. The likelihood of NOx formation could be prevented in a hydrogen-transfer SOFC. We would have chosen an SOFC of this configuration if there was one commercially available. Also, NOx monitoring at the significant level was not performed in this study.

Materials and Methods

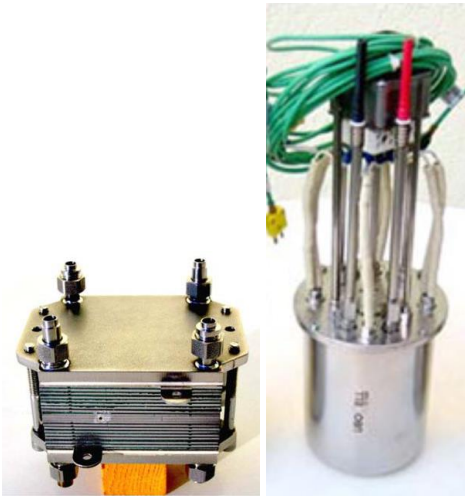

a) Stack only b) SOFC "module"

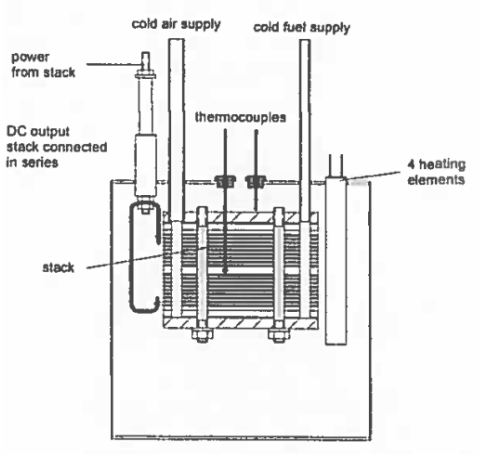

c) SOFC "module" schematic

Fig. 3. Supplier's images of SOFC stack [12].

The starting point for the REACH design was finding a commercially available SOFC stack that was tolerant to ammonia. Figure 1a shows the SOFC stack we bought that was designed to operate at 700ºC, with a nominal power rating of 100W. It is worth noting that, as we bought it, this stack was only operable with constant electrical heat input from four 125W cartridge heaters (500W total) in the 'module' configuration we had ordered (see Fig. 3c). We reused the same four 125W cartridge heaters in REACH for initial heating.

Table 1. SOFC stack supplier's specification.

Dimensions L x W x H	60 mm x 60mm x 40mm (2.37" x 2.37" x 1.58")
Number of cells:	16
Performance (700°C):	OCV ≈ 17 V, N = 80 W at 12 V for H2 and air
Type of cell:	0.4 mm anode-supported, anodes reduced before stack assembly
Cell material:	Anode. Ni-Cermet, electrolyte: ZrO, cathode: LSM
Bipolar and end plates:	1 mm Crofer 22, with etched flow fields
TC center plate:	4 mm Crofer 22 for placement of one thermocouple near stack center
Compression plates:	4 mm stainless steel: 316L or 1.4305
Electrical insulation:	1 mm Al2O3
Start-up time:	60 minutes inside furnace
Endurance:	More than 100 hours and more than 20 cycles

A simple energy accounting approach based on the maximum DC power out of the SOFC was used as a basis for design,

$$Calorific\ Power\ In = Power\ Out + Losses$$

We assumed that the heat exchanger with integrated cracker would manage 100% cracking of the ammonia, which allowed us to consider the hydrogen flow rate through the SOFC, with parameters from Table 2.

The manufacturer's typical performance at 700ºC is shown in Fig. 4, we used this to find the maximum DC power out of the SOFC.

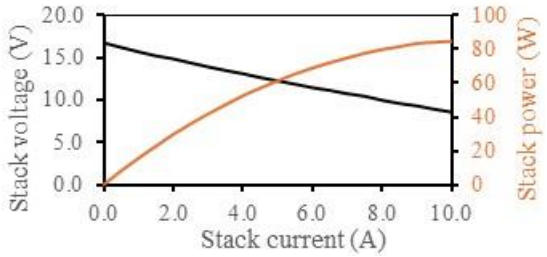

Fig. 4. Manufacturer's performance data at 700ºC [12].

Table 2. Assumed SOFC parameters.

SOFC Parameter	Value
Efficiency, η_{SOFC}	0.5
Conversion effectiveness, ε_{SOFC}	0.85
Maximum DC out, $P_{DC\ MAX}$	85 W

Constant	Value
Δh_{crack}	46.4 kJ/mol
$x_{O_2}^{[air]}$	0.21
M_{H_2}	2 g/mol
M_{N_2}	28 g/mol
M_{NH_3}	17 g/mol
M_{air}	29 g/mol

For the SOFC boundary,

$$\dot{E}_{H_2} = P_{DC} + \dot{Q}_{SOFC} + \dot{E}_{H_2\ residual} \quad (1)$$

The rate of hydrogen conversion for a given DC power output,

$$P_{DC} = \eta_{SOFC}\dot{E}_{H_2\ converted} \quad (2)$$

From the rate of hydrogen conversion, the heat produced in the SOFC can be determined using:

Table 3. Power balance for 85W operating point of SOFC.

Variable	Power (W)
$\dot{E}_{H_2\ converted}$	170
$\dot{Q}_{SOFC}$	85
$\dot{E}_{H_2\ residual}$	30

$$\dot{Q}_{SOFC} = (1 - \eta_{SOFC})\dot{E}_{H_2 converted} \quad (3)$$

The conversion effectiveness of the SOFC can then be used to calculate the total calorific rate of hydrogen that must be entering to facilitate a given operating point,

$$\dot{E}_{H_2\ converted} = \varepsilon_{SOFC}\dot{E}_{H_2} \quad (4)$$

And finally, the residual hydrogen, not processed by the SOFC,

$$\dot{E}_{H_2\ residual} = (1 - \varepsilon_{SOFC})\dot{E}_{H_2} \quad (5)$$

Table 3 shows the residual fuel that could be captured by a post SOFC combustor. The combustor is important to maximise the available heat budget but also an obvious addition so as not to waste 15% of the fuel out of the exhaust, especially given the toxicity of ammonia and the global warming potential of hydrogen. We assume the combustor is 100% efficient with no residual fuel left over ($\dot{Q}_{SOFC} = \dot{E}_{H_2\ residual}$), which allows us to amend Eq. (1) to the following,

$$\dot{E}_{H_2} = P_{DC} + \dot{Q}_{SOFC} + \dot{Q}_{comb} \quad (6)$$

From the required calorific rate of hydrogen, we can derive a flow rate and the output conditions of a cracker. The LHV of hydrogen was used to obtain a conservative hydrogen flowrate into the SOFC; using the HHV would result in a lower flowrate and therefore a lower cracking endotherm,

$$\dot{m}_{H_2} = \frac{\dot{E}_{H_2}}{LHV_{H_2}} \quad (7)$$

The molar flowrate of hydrogen is,

$$\dot{n}_{H_2} = \frac{\dot{m}_{H_2}}{M_{H_2}} \quad (8)$$

The ammonia cracking reaction is,

$$NH_3 + 46.4\ kJ \rightarrow 0.5\ N_2 + 1.5\ H_2 \quad (9)$$

Therefore, from the cracking reaction, the required ammonia flow rate is,

$$\dot{n}_{NH_3} = \frac{\dot{n}_{H_2}}{1.5} \quad (10)$$

$$\dot{m}_{NH_3} = M_{NH_3}\dot{n}_{NH_3} \quad (11)$$

The endotherm heating rate requirement is given by,

$$\dot{Q}_{crack} = \dot{n}_{NH_3} \times \Delta h_{crack} \quad (12)$$

Now we have all of the terms required to express the thermal power balance for the system,

$$\dot{Q}_{SOFC} + \dot{Q}_{comb} = \dot{Q}_{crack} + \dot{Q}_{loss} \quad (13)$$

Equation (13) shows the budget from which the cracking endotherm must be satisfied, whilst suffering the inevitable losses from the heat exchanger's exhaust and through the thermal insulation and vessel to the atmosphere. Note that because the preheating endotherm is met by heat exchange with the exhaust gases, there is not a preheating term in Eq. (13). The tolerable heat

loss rate would be shared between the exhaust gases and the losses through the walls,

$$\dot{Q}_{loss} = \dot{Q}_{walls} + \dot{Q}_{exhaust} \quad (14)$$

Table 4. Thermal power balance results for 85W operating point.

Variable	Thermal Power (W)
$\dot{Q}_{comb}$	30
$\dot{Q}_{SOFC}$	85
$\dot{Q}_{crack}$	21.8
$\dot{Q}_{loss}$	93.3

The tolerable losses were predicted to be 93.3 W, Table *4*, result here indicated that the concept was worth pursuing, and on this basis the design of REACH begun. The relative magnitudes of $\dot{Q}_{walls}$ and $\dot{Q}_{exhaust}$ were to be determined following some more design effort.

The corresponding air flow rate requires the introduction to the SOFC's conversion chemical reaction,

$$H_2 + O^{2-} \rightarrow H_2O + 2e \quad (15)$$

The air flow rate, or more specifically the air-fuel equivalence ratio (AFR), is an important variable of the REACH design. Because Eq. (15) for the SOFC is strongly temperature dependent, varying the AFR was the way in which we wanted to control the temperature of the SOFC. The minimum AFR we would choose to run at is 1.0, which is the stoichiometric oxygen flow rate, and the maximum was thought the be about 10.0. The stoichiometric oxygen flow rate for this fuel flow rate is given by,

$$\dot{n}_{O_2@AFR=1} = \frac{\dot{n}_{H_2}}{2} \quad (16)$$

The molar fraction of oxygen in dry air, $x_{O_2}^{[air]}$, is 0.21. Therefore, the minimum air flow for this fuel flow rate is,

$$\dot{n}_{air@AFR=1} = \frac{\dot{n}_{O_2}}{x_{O_2}^{[air]}} \quad (17)$$

$$\dot{m}_{air@AFR} = AFR \times M_{air}\dot{n}_{air} \quad (18)$$

The maximum AFR we anticipated was AFR=10.0. We assumed the cracker would achieve 100% cracking. The nitrogen flow rate from the cracker,

$$\dot{n}_{N_2} = \frac{\dot{n}_{NH_3}}{2} \quad (19)$$

$$\dot{m}_{N_2} = M_{N_2}\dot{n}_{N_2} \quad (20)$$

Table 5. Molar flowrates for 85W operating point.

Molar Flow Rates	Value (mol/s)
$\dot{n}_{H_2}$	8.35×10^{-4}
$\dot{n}_{NH_3}$	4.70×10^{-4}
$\dot{n}_{N_2}$	3.53×10^{-4}
$\dot{n}_{O_2@AFR=1}$	4.175×10^{-4}
$\dot{n}_{air@AFR=1}$	1.99×10^{-3}
$\dot{n}_{air@AFR=10}$	1.99×10^{-2}

Table 6. Mass flow rates for 85W operating point.

Mass Flow Rate	Value (g/s)
$\dot{m}_{H_2}$	0.00167
$\dot{m}_{N_2}$	0.00988
$\dot{m}_{NH_3}$	0.00799
$\dot{m}_{air@AFR=1}$	0.0577
$\dot{m}_{air@AFR=10}$	0.577

Heater Exchanger with Integrated Cracker Feasibility

The cracker was the central channel of a triple tube heat exchanger, starting halfway along the length. Ruthenium on alumina pellets were the chosen cracking catalysts because they fitted inside the central tube and a previous experiment had shown very high conversion at the intended operating temperature [13]. A steady-state model was built in ANSYS including the cracking reaction. Fig. ***5*** shows the steady state results and how the length of the heat exchanger was broken into a cracking portion and a preheating portion. An AFR of approximately 7.0 was chosen for this study. For this model, the geometry was assumed to be linear, and the other assumptions are listed in Table *7*.

Table 7. CFD model inputs/assumptions

Parameter	Value	Units
Fuel pre heat length	1.5	m
Cracker length	1.5	m
Air/exhaust exchanger length	3	m
Fuel ID	4	mm
Exhaust ID	5	mm
Exhaust OD	9	mm
Air ID	10	mm
Air OD	12	mm
Mass flow air	0.5	g/s
Mass flow exhaust	0.5	g/s
Mass flow ammonia	0.01	g/s
AFR	6.93	
Air inlet temp	20	ºC
Exhaust inlet temp	849	ºC

Fuel preheat inlet temp	20	ºC
Catalyst pellet diameter	3	mm
Catalyst material	Ruthenium on alumina	

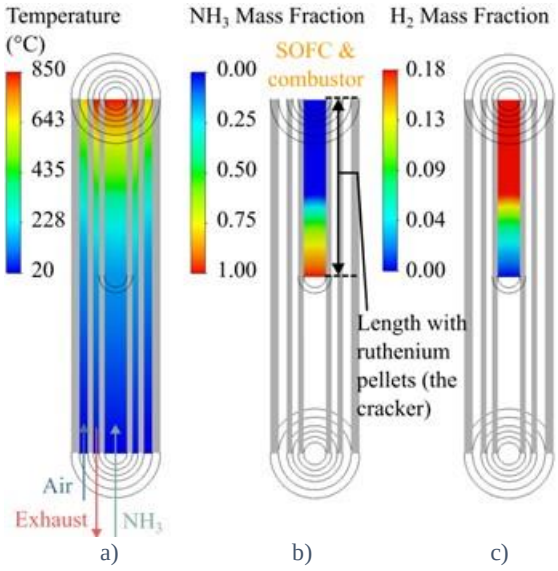

Fig. 5. CFD study of the cracker design.

Table 8. Cracker CFD model results.

Result	Value	Units
Air outlet temp	676	ºC
Exhaust outlet temp	99	ºC
Heat transferred to air	329	W
Fuel preheat outlet temp	339	ºC
Cracker outlet temp	642	ºC
Heat transferred to fuel preheat	8	W
Heat transferred to cracker	41	W

The CFD results (see Table 8) gave us confidence to proceed with the concept and return to the tolerable thermal loss. Because the air mass flow rate is so much higher than that of the fuel, the exhaust temperature loss can be approximated by,

$$\dot{Q}_{exhaust} = \dot{m}_{air} c_{p\,air} (T_{exhaust} - T_{amb}) \quad (21)$$

The CFD boundary conditions and results were used in Eq. (21), then Eq. was evaluated for the tolerable wall losses, yielding the results shown in Table 9. Most of the tolerable thermal loss was therefore to be addressed by insulation design.

Table 9. Breakdown of thermal losses $\dot{Q}_{loss}$ for 85W operating point.

Loss Term	Thermal Power (W)
$\dot{Q}_{exhaust}$	39.7
$\dot{Q}_{walls}$	53.6

Preliminary Design

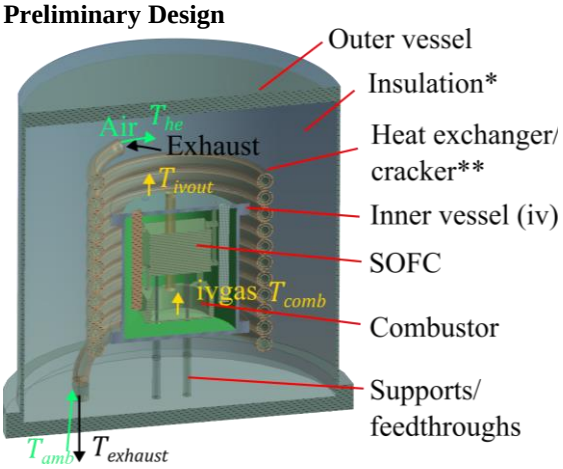

Fig. 6. Overview of the geometry and setup of the ANSYS CFX model of the preliminary design. *Insulation is hidden for clarity but filled all the void space. ** The inner wall of the cracker was not included.

Fig. ***6*** shows the setup of the steady-state CFD model we used to assess our preliminary design (see Fig. 1 and Fig. 2) against the thermal loss requirement. This was an iterative process that led to the replacement of radiation shielding in the evacuated chamber with a solid-state microporous insulation (compare Fig. 2 and Fig. 10). The preliminary design CFD model was built to see whether our design could sustain cracking while accounting for realistic thermal losses. To simplify the physics the following assumptions were made,

- The fuel in line, and thus the cracking reaction, was represented as a non-uniform heat flux with the profile shown in Fig. 7, taken from an iteration of the cracker CFD model.
- The SOFC and combustor's internal geometry was ignored. A heat generation rate over the volume of the SOFC and the combustor's outlet temperature was used to govern the overall thermal input to the system.

$$T_{comb} = \frac{\dot{Q}_{SOFC} + \dot{Q}_{comb} + \dot{m}_{air} * c_{p\,air} * (T_{he} - T_{amb})}{\dot{m}_{ivgas} * c_{p\,air}} + T_{amb} \quad (22)$$

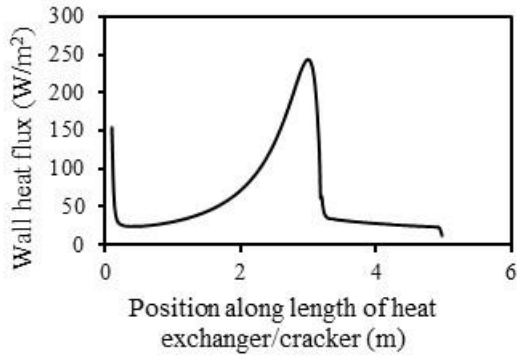

Fig. 7. Wall heat flux profile used to represent the cracking endotherm in the preliminary design CFD study.

- The inner vessel gas was linked by equation to the heat exchanger channels rather than modelling the full geometry of mixing flows, where,

$$\dot{m}_{ivgas} = \dot{m}_{exhaust} \quad (23)$$

$$\dot{m}_{ivgas} = \dot{m}_{air} + \dot{m}_{NH_3} \quad (24)$$

- All gas domains (air line, exhaust line and inner vessel gas) were modelled as air.
- All solid domains were modelled at steel, with the exception of the insulation which was modelled with the material properties of Promat's Microtherm insulation [14].

Table 10. Boundary conditions of the preliminary design CFD study.

Parameter	Value	Units
SOFC utilisation	0.85	
SOFC conversion efficiency	0.5	
Calorific Rate In	235.3	W
DC power out	100	W
Unreacted H2	35.3	W
Total thermal power in	135.3	W
Ambient temperature	27	C
Air flowrate	0.9	g/s
Fuel	0.011	g/s
Air fuel equivalence ratio	11.2	
Cracking endotherm	30.3	W
Inner vessel gas	0.911	g/s
Exhaust gas	0.911	g/s
Thermal conductivity of steel	15	W/mK
Thermal conductivity of Microtherm insulation	0.022	W/mK

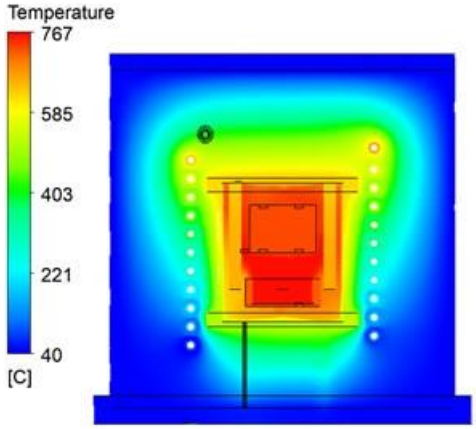

Fig. 8. Steady state CFD result: section view of REACH.

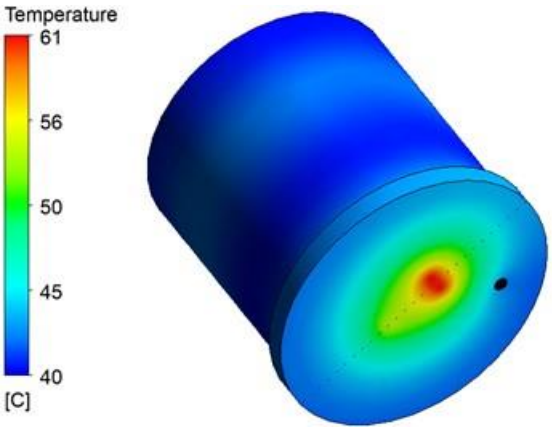

Fig. 9. Steady state CFD result: outer vessel hot spots.

For the last iteration, shown in Fig. 8 and Fig. 9, the key results are shown in Table 11.

Table 11. Key results from preliminary design CFD study.

Result	Value	Units
Thermal input inferred	133.0	W
Overall wall heat loss rate	39.2	W
Exhaust gas loss	59.0	W
Heat available for cracking	37.1	W

As Fig. 9 shows, there is an unavoidable hot spot where the feedthrough supports meet the outer vessel base due to conduction. The preliminary CFD model successfully demonstrated that the cracking requirement was met despite losses through the exhaust and through the walls. Therefore, it provided a design which we were happy to proceed with, and a resource against which to benchmark the testing.

Final Design

From the core outwards (see Fig. 10) the mechanical design of REACH was as follows: the 100W SOFC with catalytic combustor mounted below; an inner vessel offering electrical heating and creating a gas-tight environment for the SOFC and combustor; a helical triple-tube heat exchanger and cracker wrapped around the inner vessel conveying air, fuel and exhaust gas to and from the inner vessel; an outer vacuum vessel with Promat insulation; a mechanical frame housing the controller, gas supply interfaces, fuel and air shut-off valves, communications sockets and the electrical take-offs from the fuel cell. This outer frame had its own ventilation, to guarantee an ATEX zoning of negligible extent and therefore avoid the need for ATEX rated electronics inside the frame.

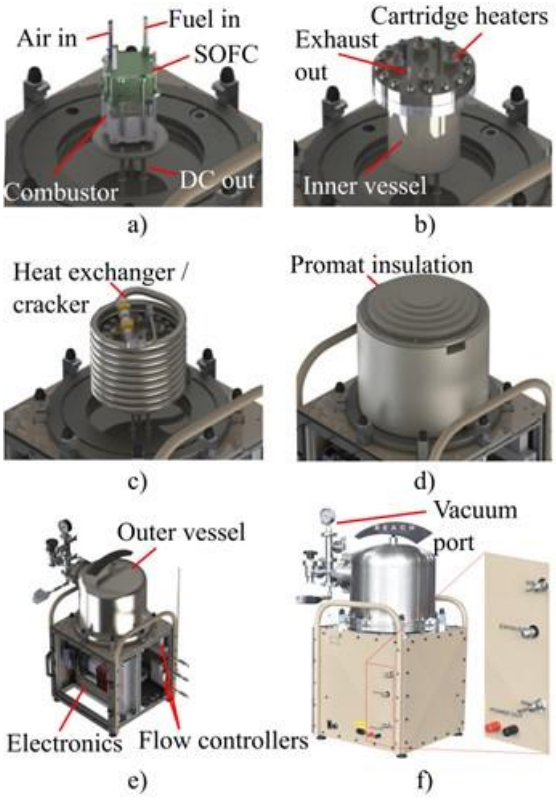

Fig. 10. Staged assembly CAD renders (a-e) with photo of final build (f).

The instrumentation is best explained in the *Supplementary Material*, Fig. 22). The control software was built in NodeRed and executed by a Groov Rio. There was also a hardwired safety circuit with emergency stop capability which would automatically shut off the fuel supply, air supply and open the output circuit to prevent the flow of current. The triggers for the safety trip were the following,

- Combustor overtemperature
- Fuel cell overtemperature
- Loss of vacuum in outer vessel
- Emergency stop button.

We built a graphical user interface for the control software which displayed live data such as: process temperatures and current and voltage from the SOFC. The final control of REACH was partially manual and partially automated. The fuel rate was set through the software which linked to a mass flow controller, whereas the air flow rate was controlled by hand using a needle valve. Here, the software measured the air flow rate using a mass flow meter and gave an indication of the AFR. Note that REACH required its fuel and air supplies to be at slightly above atmospheric pressure, as it contains no internal pumps.

The electrical heating was feedback controlled to achieve an SOFC temperature setpoint. This controller was always active, so that electrical heating would automatically be used if necessary. Therefore, the user could send fuel and air into the SOFC and this would take over from the electrical heating, without needing to turn the controller off. The build was completed for testing in early 2023, and Fig. 11 outlines some of the major the stages of assembly.

Fig. 11. Staged build of the REACH prototype.

Laboratory Set Up

The assembled REACH was placed inside a fume hood on a table (see Fig. 12) and connected to laboratory gas supplies. The vacuum port was connected to a vacuum pump. The testing configuration is provided in further detail in the supplementary material (Fig. 22). A mass spectrometer was used to sample the exhaust stream. Before testing began, reduction of the anode with

hydrogen occurred until we saw the open circuit voltage we expected.

The REACH testing program consisted of the following tests:

1. *Start up* to autothermal operation on ammonia.
   i. While flowing argon down the fuel and air lines, allow the electrical heating controller to elevate the SOFC temperature to 600 °C.
   ii. Start flowing ammonia and air in rather than argon and wait for the electrical heating controller to drop off.
2. *Fuel switchover*,
   i. While operating at steady conditions, switch between ammonia supply, the equivalent hydrogen flow rate.
3. *Performance mapping* with ammonia
   i. While at operating temperatures,
      - Select a fuel rate,
      - Select an AFR,
      - Sweep the resistance of the DC load
      - Repeat ii and iii until the desired range of AFRs has been covered.
      - Repeat ii, iii and iv until the range of fuel rates has been covered.
4. *Smartphone charging demo*.
   i. Replace the programmable DC load with an inverter with a mains socket
   ii. Plug a smartphone in and allow to charge

Fig. 12. REACH in the laboratory during testing.

Results and Discussion

The testing data for REACH is available upon request from the author. Fig. 13 is provided to help with the interpretation of the following results.

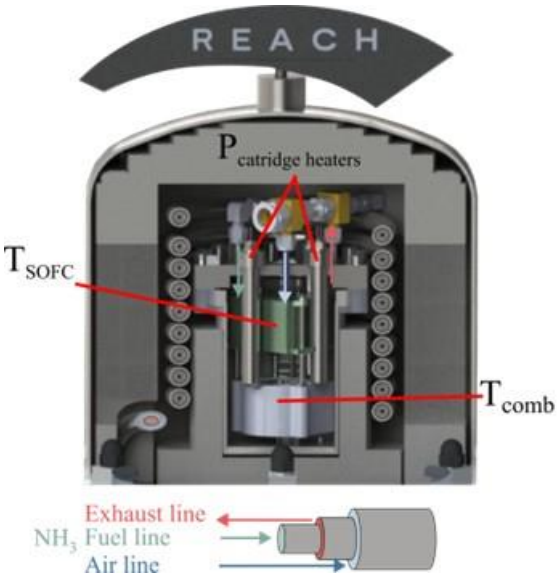

Fig. 13. Rendered and labelled cutaway view of REACH.

Start Up Results

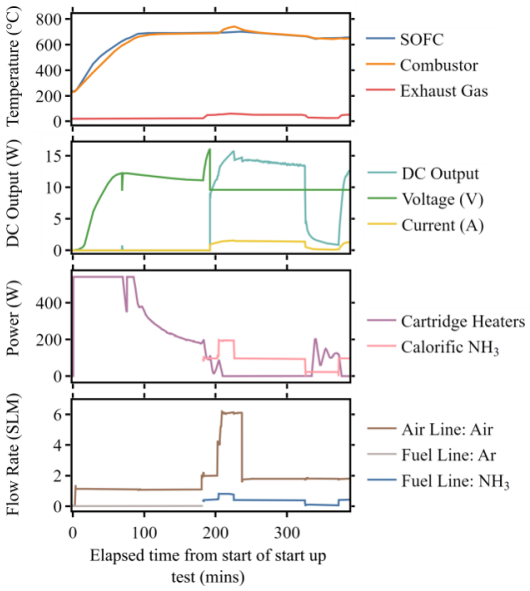

Fig. 14. Start up test results.

In Fig. 14, the injection of ammonia starts where the "calorific rate of NH_3" trace starts. Before this point REACH is being heated electrically with Argon flowing through the fuel line, and we can see the electrical power consumption dropping as the setpoint SOFC temperature of 650°C was approached. Note the open circuit voltage forming due to the temperature. Following injection of fuel, see the rise in open circuit voltage to 16V, just before the power output becomes non-zero. From this point onwards during the test, it is evident that the system is autothermal due to the absence of heating input.

The small period with electrical heating after 300 minutes is due to a reduced fuel rate, as we prepared for the performance mapping tests. At the end of the data shown in Fig. 14, the electrical heating power drops away to zero again under a steady fueling condition shown in Fig. 15.

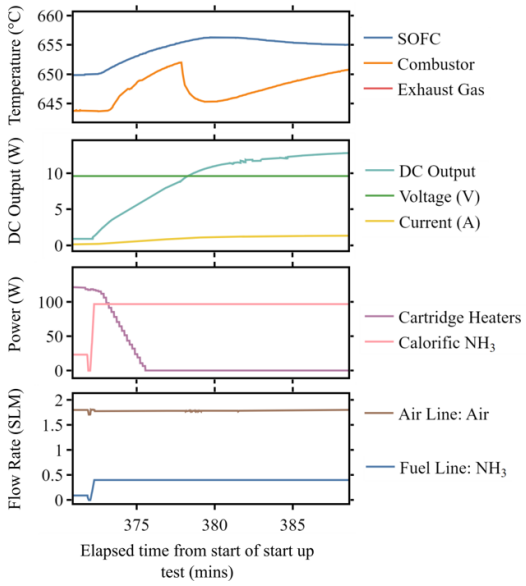

Fig. 15. Zoomed view of the end of the start-up testing.

This is highlighted in case the slight negative gradient of temperatures (caused by an initial boost to the fuel rate) during the initial fuel injection period casted doubt over the autothermal capacity of the system.

Fuel Switchover Results

To prove that REACH was robust to hydrogen and ammonia fueling the equivalent calorific rates were fed of both fuels in one testing session on a separate testing day. Figure 16 shows the performance was very similar. It also serves to prove that the cracker was achieving near 100% decomposition.

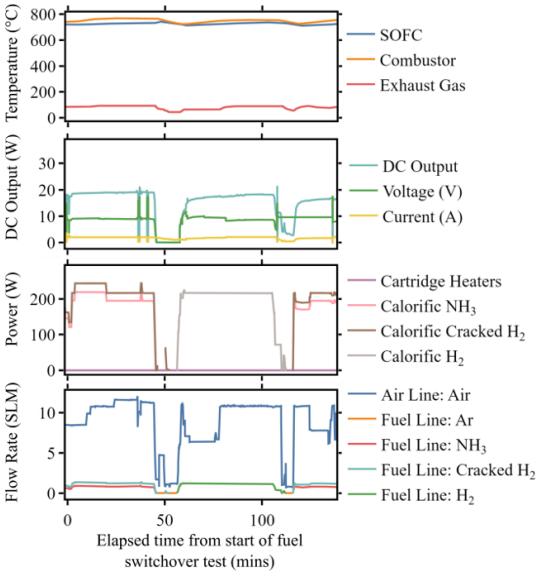

Fig. 16. Fuel switchover results.

Performance Mapping with Ammonia

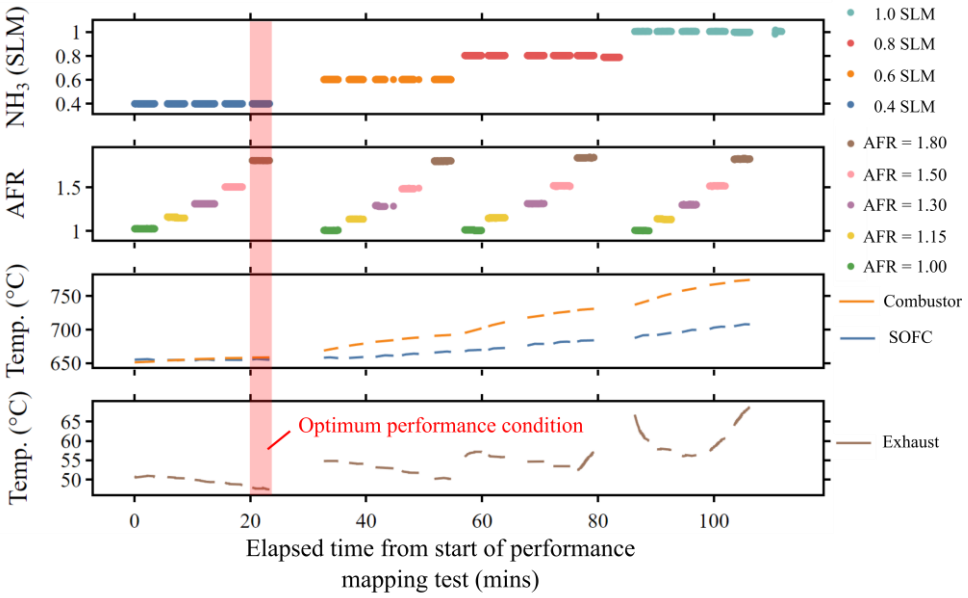

Fig. 17. Dataset slices behind performance mapping.

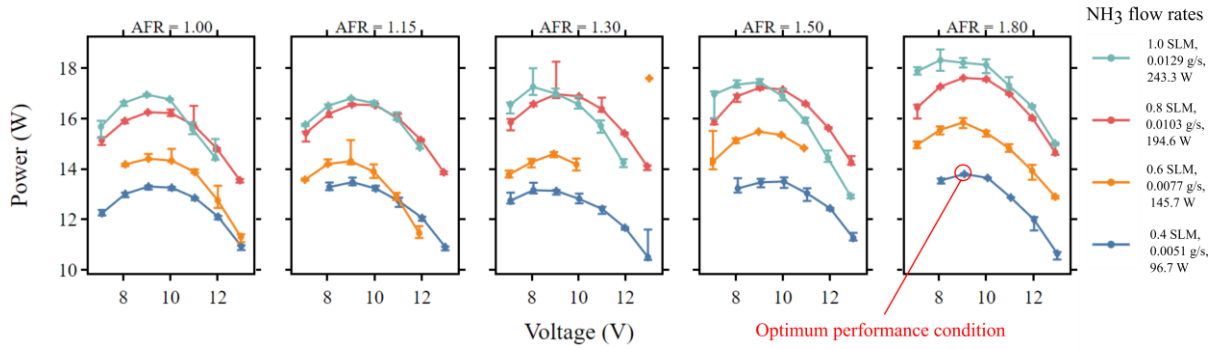

Fig. 18. Performance mapping DC Power out against SOFC voltage.

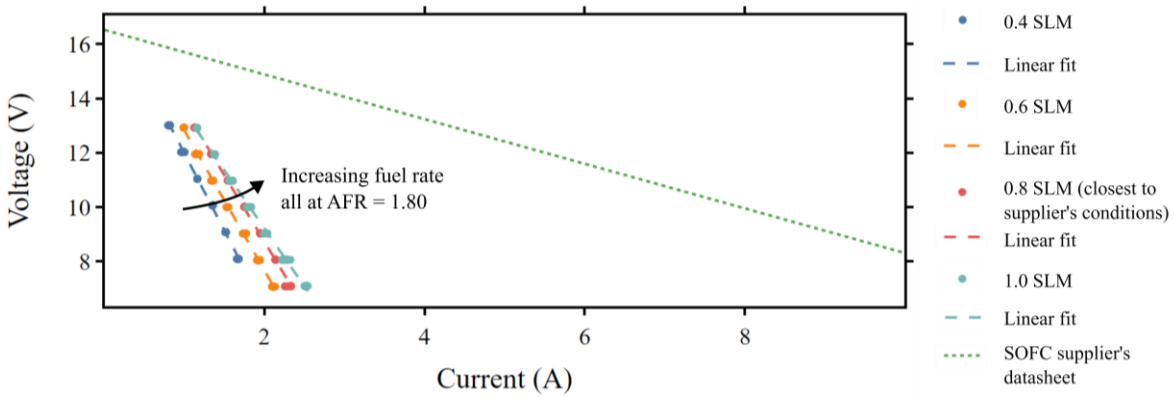

Fig. 19. Voltage vs current performance versus the supplier's data.

The performance mapping was conducted under autothermal conditions, in fact it immediately followed the start-up testing on the same day. Fig. **19** shows the characteristic shape expected of a fuel cell with an optimum supply voltage of around 9V. When comparing the traces, the power output increases for higher fuel rates as anticipated. However, this effect is much smaller than anticipated, indicating a conversion issue within the SOFC. Note the especially small power output increase when moving from 0.8 SLM and 1.0 SLM, indicating a saturation behavior at much lower fueling rates than expected. Referring to Fig. 17, it can be argued that it is an increased temperature effect that is driving the power increase rather than simply converting more fuel because more is available. Furthermore, Fig. 17 illustrates the relationship between the SOFC and combustor. The combustor temperature rising above the SOFC temperature occurs when the fuel is being burned rather than converted in the SOFC. This had not been the design intention, and the reason we operated in this region was because we were trying to obtain the IV curve stated in the manufacturer's data. Therefore, it was deduced after testing that 0.4 SLM of ammonia was about the limit of what the SOFC could convert and thus our performance metric is taken from this region of the data (see red highlights on Fig. 17 and Fig. 18). We present Table 12 as the key metrics from REACH.

Table 12. Optimum performance condition results.

Condition	**Value**			
Air flowrate	3.141 (SLM)	0.0668 (g/s)	2.30E-03 (mol/s)	
NH_3 flowrate	0.399 (SLM)	0.0051 (g/s)	3.01 E-04 (mol/s)	96.7 (W)
Equivalent H_2 flowrate	0.599 (SLM)	0.0009 (g/s)	4.49 E-04 (mol/s)	107.6 (W)
AFR	1.81			
T_{SOFC} (°C)	656.0			
T_{COMB} (°C)	658.2			
T_{EXH} (°C)	47.71			
V_{SOFC} (V)	9.08			
I_{SOFC} (A)	1.52			
P_{DC} (W)	13.80			
System Efficiency	14.26 %			

To interpret the results of Table 12, we revisited the calculations from the method section of this paper, and used the SOFC reaction equation to back

calculate the SOFC utilization and efficiency; the parameters we had initially had to assume would match those of literature.

Table 13. Predicted vs actual at optimum operating point.

Result	Expected	Actual
NH_3 flowrate (W)	96.7	96.7
H_2 eq. flowrate (W)	107.6	107.6
P_{SOFC} (W)	45.7	13.8
$\dot{Q}_{SOFC}$ (W)	45.7	16.4
$\dot{Q}_{comb}$ (W)	16.1	77.4
$\dot{Q}_{crack}$ (W)	14.0	14.0
$\dot{Q}_{loss}$ (W)	47.9	79.9
SOFC Utilisation (%)	85.0	28.1
SOFC Efficiency (%)	50.0	45.6
System Efficiency (%)	47.3	14.3

It was found that the SOFC had a much lower utilization than expected (see Table 13). This was the key driver of the low system efficiency and led to most of the calorific content being converted in the combustor rather than in the SOFC, more heat being generated and consequently the rate of heat loss was higher than expected. There was evidently a fault with this SOFC according to the expectations its datasheet gave us (see Fig. 4). It remained to see if the REACH system had damaged the SOFC in some way, or whether there was a manufacturing problem. To resolve this, REACH was stripped down and the SOFC sent back to the manufacturer (see Supplementary Information for post testing photos). The manufacturer conducted hydrogen tests in a furnace in their laboratory on the same SOFC stack and confirmed that indeed the SOFC could not produce more than around 30 W, even after refurbishment. A test was also conducted with other stock SOFCs with the same result, concluding that the issue was not caused by REACH. The SOFC was also taken apart and inspected by the supplier. No structural damage to the SOFC was observed, leading to the primary suspected cause of the poor fuel cell performance being an incorrect reduction process; 10% H_2, 90% Ar or He should be used, whereas 100% H_2 at low flow rates and low pressure for an extended period was used instead. According to Grahl-Madsen *et al.*, sintering of the anode can occur during the reduction process if it takes place at lower temperature. A slow lower temperature reduction process could significantly impair the electrical conductivity of the anode [15]. In a future incarnation of this ammonia driven SOFC system, we would reduce the anode ourselves using the appropriate gas mixture and following guidelines on reduction temperature and rate rather than procuring an SOFC stack with pre-reduced anodes to mitigate risk that this sensitive process is not done correctly.

Despite the setback of reduced system efficiency, the thermal design of REACH was robust to this far from optimal condition and the integrated heat exchanger and cracker was proved to be very successful in practice. The insulation design was also successful because electrical heating was not necessary to maintain the system operation.

Charging Demo

Before the system was disassembled, REACH was configured to deliver power for a "real-world" application. For the charging demonstration, an inverter and a battery charge controller were installed over the terminals of the programmable load. Evidence is provided in Fig. 20 of a smartphone being charged. This demonstration showed that we were able to charge a smart phone from ammonia using REACH, which while not leading to any further technical conclusions, was a good final test to complete the story of this prototype and illustrate a small real-world application of IA-SOFCs.

Fig. 20. Photo of REACH being used to charge a smartphone.

Conclusions

A novel IA-SOFC system design called REACH was modelled, built and tested in which the operating conditions were maintained auto thermally from waste heat, supplying the cracking endotherm from waste heat and unspent fuel in the outlet of the SOFC. The predicted efficiency of this system, from calorific flow rate of ammonia in to DC power out, was expected to be 47%. However, we were only able to achieve 14.3% in this build due

to the bought in SOFC having a much lower utilisation (28.1% rather than 85%) than anticipated. Thus, the autothermal ability of the system was more from unspent fuel than from waste heat in this instance. SOFC maturity and commercial availability significantly held back the performance of this prototype and highlighted the potential sensitivity of the anode reduction process. However, the authors are confident that the CFD and first principles modelling show that the REACH system could deliver 47% system efficiency if the SOFC were to perform in line with the literature.

Despite this SOFC performance setback, the design was shown to be robustly autothermal, and practically demonstrated an IA-FC system with no filtering step. A triple channel heat exchanger cracker underpinned the success of the project and was able to achieve preheating of the fuel and air and near 100% cracking. A fuel switch over was demonstrated, where switching from ammonia to the equivalent hydrogen flowrate achieved the same performance.

The suggested next steps are to scale up to the 1-10kW power rating with a reliable SOFC stack and conduct a detailed look at the exhaust composition. A further improvement would be to remove the vacuum insulation from the design as this required a vacuum pump to be continuously operating. The larger scale presents less of a challenge thermally and the prototype at this scale has demonstrated a promising basis for design.

Acknowledgments

The authors of this paper would like to thank Business Innovation and Development (BID) at STFC for funding the project. the workshop staff at the Rutherford Appleton Laboratory for their skill and support with the manufacture of many parts for REACH. It was good to have managed to design, manufacture, build and test all in one place. The authors also thank STFC, Daresbury for the electrical design and assembly behind REACH.

Conflicts of Interest

The authors declare no conflict of interest. The funders had no role in the design of the study; in the collection, analyses, or interpretation of data; in the writing of the manuscript, or in the decision to publish the results.

References

1. Rathore SS, Biswas S, Fini D, Kulkarni AP, and Giddey S. Direct ammonia solid-oxide fuel cells: A review of progress and prospects. Int J Hydro Energy 2021 46 (71):35365–35384. doi: https://doi.org/10.1016/j.ijhydene.2021.08.092
2. Jo YS, Kim HK, Johnson GR, and Montgomery MJ. Systems and methods from processing ammonia, US 2022/0389864, Dec. 08, 2022
3. Thomas G and Parks G. Potential Roles of Ammonia in a Hydrogen Economy, U.S. Department of Energy, Governmental Report, 2006. [Online]. Available in: https://www.energy.gov/eere/fuelcells/articles/potential-roles-ammonia-hydrogen-economy
4. Shabani B, Hafttananian M, Khamani S, Ramjar A, and Ranjbar AA. Poisoning of proton exchange membrane fuel cells by contaminants and impurities: Review of mechanisms, effects, and mitigation strategies. J Power Sources 2019 427:21–48, doi: https://doi.org/10.1016/j.jpowsour.2019.03.097
5. Yáñez Y, Relvas F, Ortiz A, Gorri D, Mendes A, and Ortiz I. PSA purification of waste hydrogen from ammonia plants to fuel cell grade. Sep Purif Tech 2020 240: 116334 doi: https://doi.org/10.1016/j.seppur.2019.116334
6. Peters TA, Bredesen R, and Venvik HJ. Pd-based membranes in hydrogen production: long-term stability and contaminant effects, in Membrane Engineering for the treatment of gases, 2nd Edition., RSC Publishing, 2017.
7. Guo Y, Pan Z, and An L. Carbon-free sustainable energy technology: Direct ammonia fuel cells. J Power Sources 2020 476: 228454. doi: https://doi.org/10.1016/j.jpowsour.2020.228454
8. Cinti G, Desideri U, Penchini D, and Discepoli G. Experimental Analysis of SOFC Fuelled by Ammonia. Fuel Cells 2014 14(2):221–230. doi: https://doi.org/10.1002/fuce.201300276
9. Omer A, Rahimipetroudi I, Rashid K, Yang JB, Hong JE, and Dong SK. Design and performance optimization of a direct ammonia planar solid oxide fuel cell for high electrical efficiency. J Power Sources 2023 573: 233135. doi: https://doi.org./10.1016/j.jpowsour.2023.233135
10. Kishimoto M et al. Development of 1 kW‐class Ammonia‐fueled Solid Oxide Fuel Cell Stack. Fuel Cells 2020 20(1):80‐88. doi: https://doi.org/10.1002/fuce.201900131
11. Jeerh G, Zhang M, and Tao S. Recent progress in ammonia fuel cells and their potential applications. J Mater Chem A 2021 9(2):727–752. doi: https://doi.org/10.1039/D0TA08810B
12. Bossel U, "UBOCELL SOFC Mini-Stack 'Basic.' Accessed: Feb. 15, 2024. [Online]. Available in: https://www.almus-ag.ch/products/sofc-mini-stack-basic.html
13. Cowan R, Davenne T, Huddart A, and Peters BM. HPAC: Design and testing of a high

pressure ammonia cracker, in Cracking Systems, Université d'Orléans, France, Jul. 2023.
14. Promat, "Microtherm MPS Technical Datasheet.", May 2018. [Online]. Available in: https://media.promat.com/pd36700/original/-364039941/microtherm-mps_tds_en.pdf
15. Grahl-Madsen L, Larsen PH, Bonanos N, Engell J, and Linderoth S. Mechanical strength and electrical conductivity of Ni-YSZ cermets fabricated by viscous processing. J Mater Sci. 41:1097–1107. doi: https://doi.org/10.1007/s10853-005-3647-3

Supplementary Information

A note on the CAPEX of the system. The final build of REACH cost approximately £30,000.

Supplementary Material

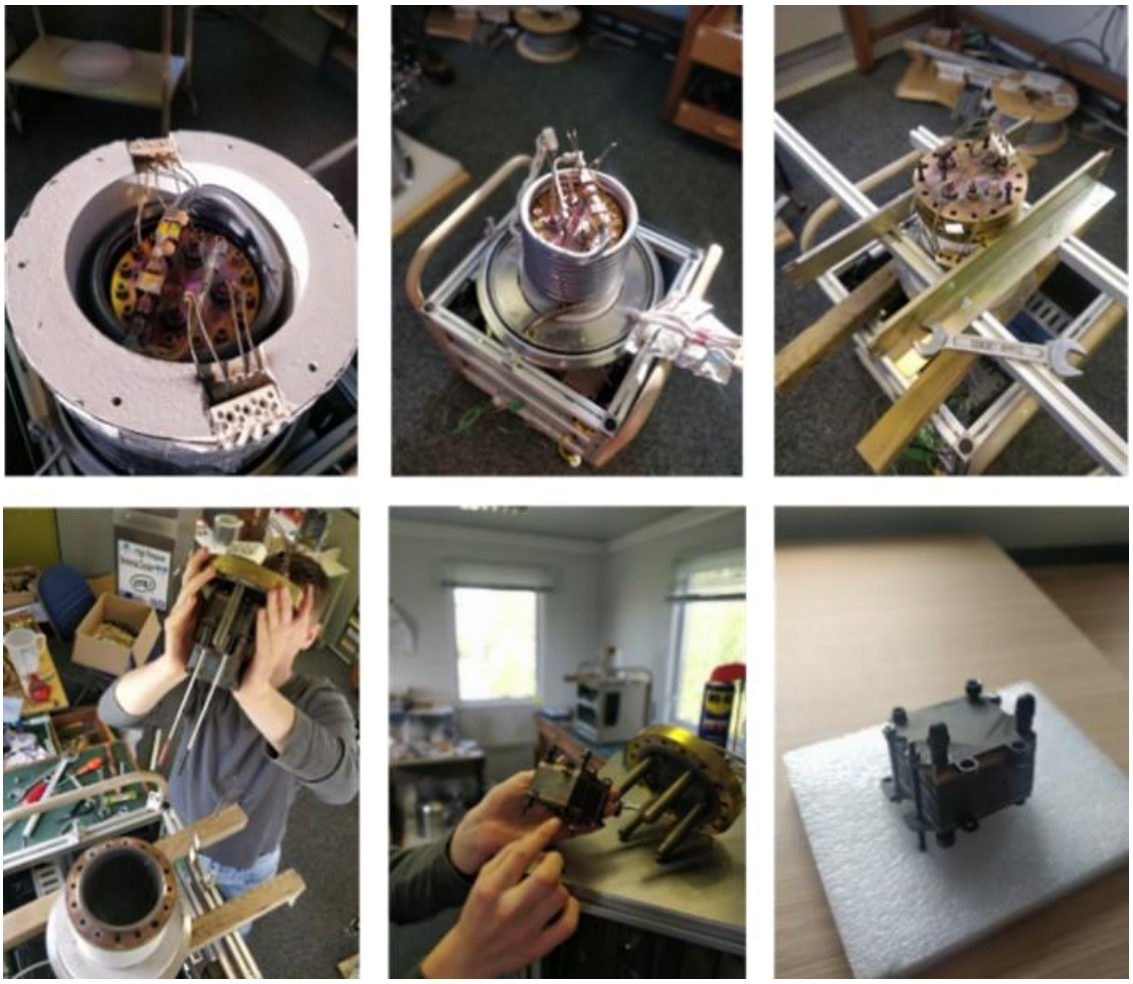

Fig. 21. Staged post-test disassembly.

1

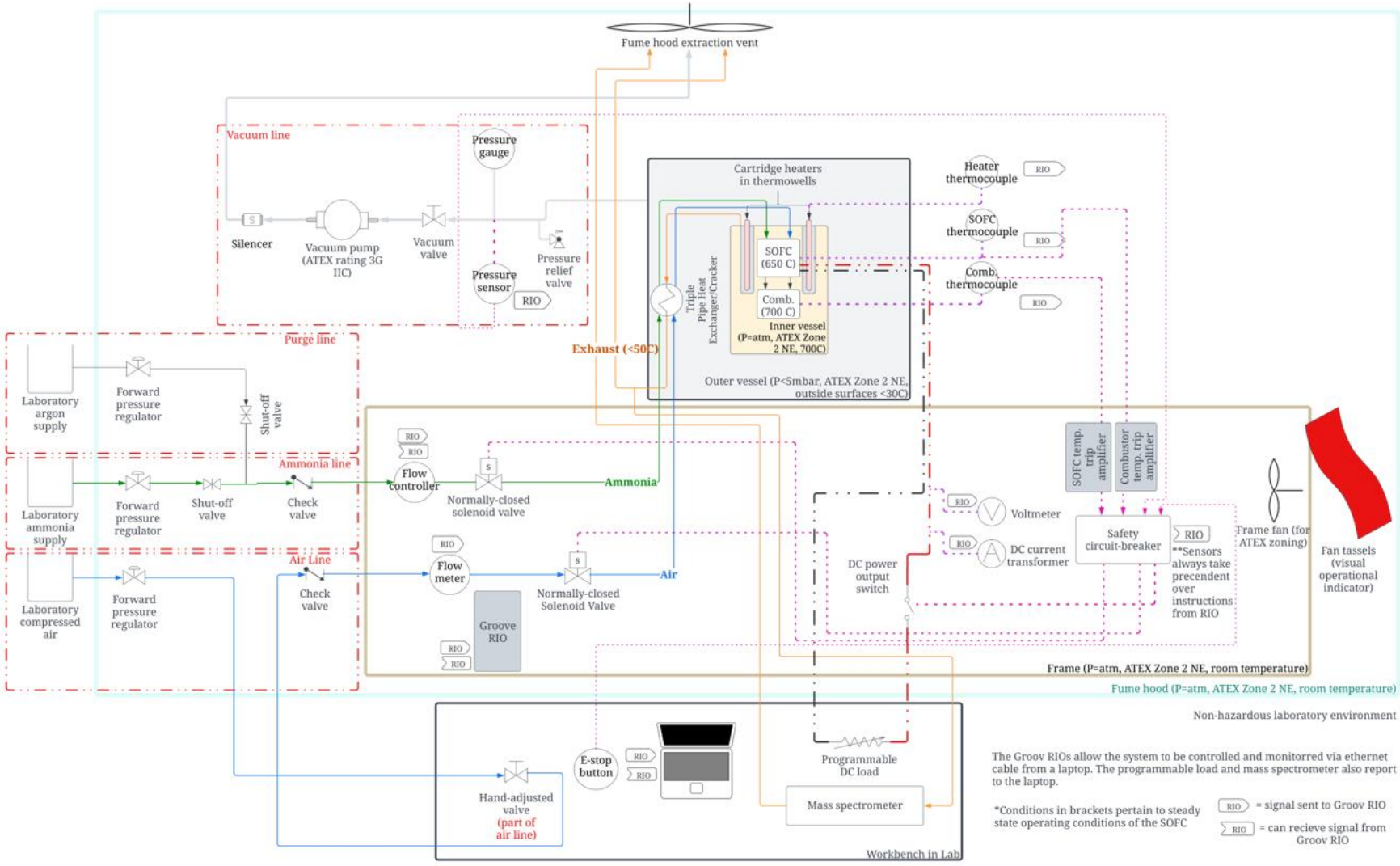

Fig. 22. Process and instrumentation diagram (P&ID) for REACH installed in laboratory.